# VVP Technique Applied to an Alberta Storm

L. XIN AND G. W. REUTER

*Department of Earth and Atmospheric Sciences, University of Alberta, Edmonton, Alberta, Canada*

19 August 1996 and 4 June 1997

ABSTRACT

The volume velocity processing (VVP) technique is used with a simulated wind field to determine the accuracy of kinematic quantities for different numbers of wind parameters and different sizes of analysis volumes. Accurate estimates of divergence, deformation, and vertical shear are obtained if the VVP method contains seven wind parameters and the analysis volumes have a range of about 20 km and an azimuthal extent of about 40°. The seven-parameter VVP method is applied to a convective storm in central Alberta, Canada. The analysis showed that low-level convergence and moderate vertical shear preceded the enhancement of precipitation, while low-level divergence suppressed the convection.

## 1. Introduction

With the increasing operational use of Doppler weather radar, there is growing interest in obtaining wind parameters from a single Doppler radar. The velocity azimuth display (VAD) analysis (e.g., Browning and Wexler 1968) has proved to be useful in estimating the profiles of mean wind and divergence over a broad area centered over the radar site. The VAD technique is suitable for widespread precipitation with considerable echo present in all quadrants of the radar. With very sensitive Doppler radars, the VAD analysis can also be performed on clear-air echoes resulting from fluctuations of refractive index of air. For convective rainfall, however, the VAD technique is of limited use because of horizontal variation of wind parameters. To deal with convective cases, the volume velocity processing (VVP) method (e.g., Koscielny et al. 1982) is appropriate. This technique divides the plane position indicator (PPI) displays into many small volumes for which the wind parameters are estimated by multivariate regression analysis. Provided that the wind field is spatially linear within each volume, wind kinematic parameters can be obtained from single-Doppler velocity data (Waldteufel and Corbin 1979). Koscielny et al. (1982) applied the VVP method and showed that areas of convergence coincided with regions where convection later developed. Smith and Rabin (1989) assessed the accuracy of this method in a case study of a severe storm outbreak in central Oklahoma.

The objectives of this note are twofold. First, we attempt to determine the accuracy of the VVP method for low-level wind conditions during convection. Using simulated velocity data, the VVP method is tested for different numbers of regression parameters. This analysis indicates the optimal setting for regression parameters to have the most accurate estimates of divergence, deformation, and shear magnitudes. The sensitivity of the VVP method on the size of the analysis volume is also determined. The second objective is to apply the VVP method for a case study of convection. The kinematic properties of the wind field are derived for a multicell hail storm that passed over central Alberta on 19 August 1992. The effect of low-level convergence and vertical shear on the storm development will be highlighted.

## 2. Number of VVP parameters and analysis volume

For the VVP analysis, radial velocity data are required in the analysis volume whose range spans from $r$ to $r + \Delta r$, azimuth from $\phi$ to $\phi + \Delta\phi$, and elevation angle from $\alpha$ to $\alpha + \Delta\alpha$ (Fig. 1). The basic assumption of the VVP method is that the spatial variation of the wind within the analysis volume $\Delta r \times \Delta\phi \times \Delta\alpha$ can be approximated by a linear function. The Doppler velocity along the radar beam $V_r$ is given by (Koscielny et al. 1982)

$$\begin{aligned} V_r &= u \sin\phi \cos\alpha + v \cos\phi \cos\alpha + w \sin\alpha \\ &= u_* p_1 + v_* p_2 + (u_y + v_x) p_3 + u_x p_4 + v_y p_5 \\ &\quad + u_z p_6 + v_z p_7 + w_o p_8 + w_x p_9 + w_y p_{10} + w_z p_{11}, \quad (1) \end{aligned}$$

where $(u_o, v_o, w_o)$ is the wind vector at the center of

*Corresponding author address:* Gerhard W. Reuter, Department of Earth and Atmospheric Sciences, University of Alberta, Edmonton, AB T6G 2E3, Canada.
E-mail: Gerhard.Reuter@ualberta.ca

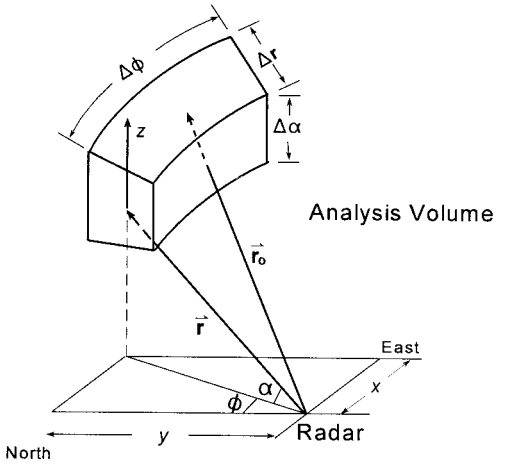


FIG. 1. Geometry of the analysis volume for the velocity volume processing technique. The $r$, $\phi$, and $\alpha$ are the radar detecting range, azimuth, and elevation angles, respectively. The range vector $\mathbf{r_o}$ is directed to the center of the analysis volume from the radar.

the analysis volume, $u_* = u_o + \frac{1}{2}y_o(v_x - u_y)$, $v_* = v_o - \frac{1}{2}x_o(v_x - u_y)$, and subscripts $x$, $y$, and $z$ denote partial derivatives. The predictor functions ($p_1, p_2, \ldots, p_{11}$) consists of trigonometric functions of $r$, $\phi$, and $\alpha$ (Koscielny et al. 1982).

The large number of radial velocity measurements within each analysis volume makes it possible to estimate the 11 model parameters in (1) using multivariate regression (see Xin 1996 for details). To reduce the variance of parameter estimates, the number of regressors can be reduced from 11, which tends to improve the confidence in the remaining parameter estimates. The VVP7 and VVP9 techniques (with 7 and 9 parameters, respectively) have been termed modified volume velocity processing (MVVP) by Koscielny et al. (1982).

To examine how the number of model parameters affects the estimates of kinematic parameters, we first apply the VVP analysis to simulated radial velocity data. To define a linear simulated wind field, the parameters $u_o$, $u_x$, $u_y$, $u_z$, $v_o$, $v_x$, $v_y$, $v_z$, $w_o$, $w_x$, $w_y$, and $w_z$ were specified using the values suggested by Waldteufel and Corbin (1979). Table 1 lists these values and compares them with their estimates using the VVP7, VVP9, and VVP11 methods. The VVP11 method seems adequate for estimation of the mean wind components $u_o$ and $v_o$, with relative errors around 30%. However, the VVP11 errors in the vertical velocity $w_o$ and the wind shear components ($u_z$, $v_z$, $w_x$, $w_y$, and $w_z$) are very large. Reducing the number of model parameters improves the results. For the VVP7 method, all estimates are fairly accurate. We have also computed the standard error of the divergence estimate $\sigma_d$ using Eq. (11) in Smith and Rabin (1989). The VVP7 technique yields a $\sigma_d = 1.5 \times 10^{-7}$ s$^{-1}$, compared to $1.5 \times 10^{-6}$ s$^{-1}$ for VVP9 and $1.4 \times 10^{-4}$ s$^{-1}$ for VVP11. These estimates show that the VVP7 technique is the most accurate for the diverge field. For the remainder of this research note, the regression model with seven parameters is used.

TABLE 1. Comparison of the estimates of kinematic parameters from the VVP7, VVP9, and VVP11 methods.

| Parameter | Units | Control | Estimates | | |
|---|---|---|---|---|---|
| | | | VVP7 | VVP9 | VVP11 |
| $u_o$ | (m s$^{-1}$) | 10 | 10.01 | 11.14 | 12.56 |
| $v_o$ | (m s$^{-1}$) | 10 | 10.05 | 12.95 | 12.94 |
| $u_y + v_x$ | ($10^{-4}$ s$^{-1}$) | 2 | 1.99 | 0.66 | 11.75 |
| $u_x$ | ($10^{-4}$ s$^{-1}$) | 1 | 1.00 | 0.96 | 1.88 |
| $v_y$ | ($10^{-4}$ s$^{-1}$) | 1 | 0.97 | 0.52 | 14.98 |
| $u_z$ | ($10^{-3}$ s$^{-1}$) | 1 | 1.008 | 14.27 | 69.5 |
| $v_z$ | ($10^{-3}$ s$^{-1}$) | 1 | 1.302 | 35.86 | −12.1 |
| $w_o$ | (m s$^{-1}$) | 5 | — | 265.3 | −4459 |
| $w_z$ | ($10^{-4}$ s$^{-1}$) | 5 | — | −17 295 | −15 219 |
| $w_x$ | ($10^{-5}$ s$^{-1}$) | 1 | — | — | 80 347 |
| $w_y$ | ($10^{-5}$ s$^{-1}$) | 1 | — | — | −17 868 |

TABLE 2. Relative errors (in percentage) of kinematic parameters estimated using VVP7 for analysis volume with sector of $\Delta\phi \times \Delta r$ and elevation span from $\alpha_1 = 0.4°$ to $\alpha_2 = 0.8°$.

| $\Delta\phi \times \Delta r$ | Relative error of VVP estimate (%) | | | | | | |
|---|---|---|---|---|---|---|---|
| | $u_o$ | $v_o$ | $u_y + v_x$ | $u_x$ | $v_y$ | $u_z$ | $v_z$ |
| 10° × 30 km | 2.8 | 0.4 | 21.0 | 127.0 | 4.0 | 30.2 | 2.6 |
| 20° × 30 km | 2.2 | 0.4 | 1.0 | 28.0 | 1.0 | 86.0 | 7.4 |
| 30° × 30 km | 1.2 | 1.1 | 0.5 | 4.0 | 1.0 | 20.6 | 20.3 |
| 40° × 30 km | 0.2 | 1.0 | 5.5 | 17.0 | 2.0 | 4.9 | 16.6 |
| 40° × 10 km | 0.6 | 1.3 | 17.0 | 32.0 | 8.0 | 3.5 | 36.4 |
| 40° × 20 km | 0.2 | 1.2 | 12.5 | 25.0 | 5.0 | 0.6 | 19.9 |
| 40° × 30 km | 0.2 | 1.0 | 5.5 | 17.0 | 2.0 | 4.9 | 16.6 |
| 40° × 40 km | 0.1 | 1.1 | 5.5 | 15.0 | 2.0 | 6.1 | 14.4 |

The VVP7 estimates are dependant on the size of the analysis volume. For different $\Delta\phi$ and $\Delta r$, the seven model parameters were computed. Table 2 compares the relative errors expressed in percentage. For all sectors shown, the estimates of horizontal mean wind ($u_o$ and $v_o$) are fairly accurate with relative errors of 10%. However, the estimates for horizontal deformation and vertical shear are quite sensitive to the variation of $\Delta\phi \times \Delta r$. In general, with the increase of $\Delta\phi$ or $\Delta r$, the accuracy decreases as a consequence of the correlations among the regressors being reduced. All seven parameters have relative percentage errors less than or equal to 25% for sector sizes of 30° × 30 km, 40° × 20 km, 40° × 30 km, and 40° × 40 km. Although larger analysis volumes contain more radial velocity measurements, the estimates obtained from such volumes become questionable due to violation of the linear wind assumption (Waldteufel and Corbin 1979). The best compromise seems to be to select an analysis volume that has an azimuthal width of about 40° and a range extent of about 20 km.

## 3. Application of the VVP technique to an Alberta storm

The seven-parameter VVP algorithm is applied to the velocity data collected by the Doppler radar at

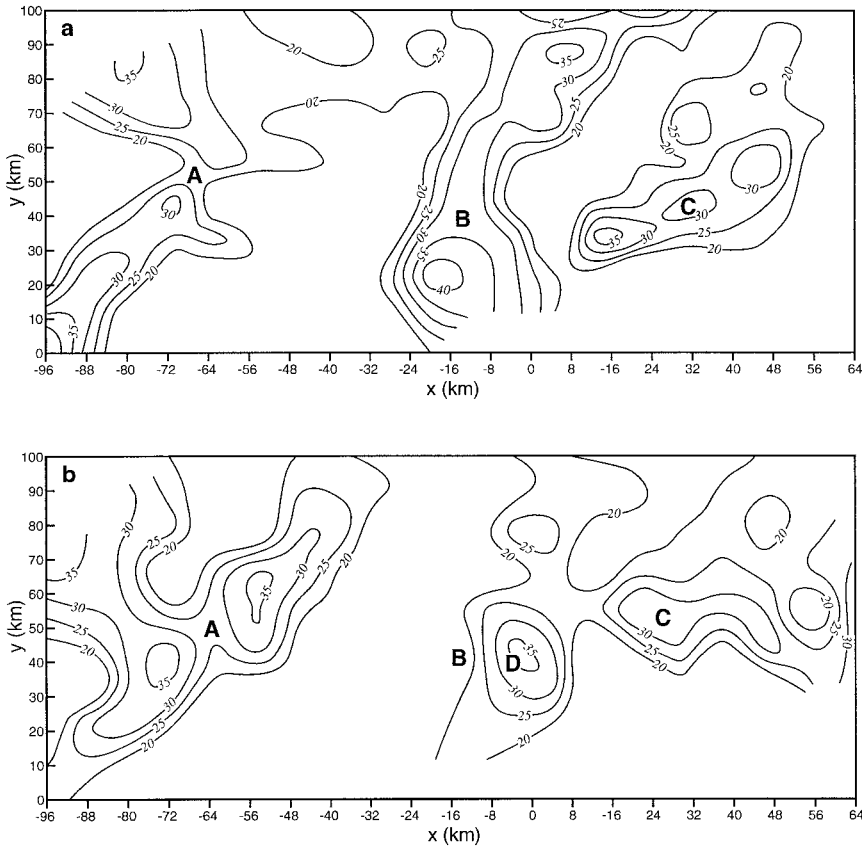


FIG. 2. Radar reflectivity PPI (dBZ) at an elevation angle of 1.5° observed at (a) 0630 UTC and (b) 0700 UTC 19 August 1992. The *x* axis points eastward with the radar sited at (0, 0). The radar echo intensity is contoured every 5 dBZ.

Carvel (53°35′N, 114°09′W) in Alberta on 19 August 1992. A shortwave trough provided favorable synoptic conditions for storm development. The leeside of the Rocky Mountains had cold air advection aloft, which contributed to the strong buildup of potential instability for convective overturning. The 1200 UTC sounding taken at Stony Plain (53°33′N, 114°06′W) indicates a dry adiabatic temperature lapse rate from the surface to about 850 mb (Xin and Reuter 1996). The air mass was convectively unstable with a convective available potential energy of about 607 J $kg^{-1}$ for the surface air. The Alberta Forestry Lightning Detection network recorded above 15 000 lightning strikes that covered a wide band of central Alberta. Pea- and golf-ball-sized hailstones were reported over many areas from 0130 to 0525 UTC. Two tornadoes damaged a mobile home and leveled trees at a campground.

Doppler velocity measurements were made by the operational C-band radar every 10 min at the elevation angles of 0.5°, 1.5°, and 3.5° within a detecting radius of 110 km. The radar technical data are given in Reuter and Beaubien (1996). Observations show that an eastward-moving multicellular storm entered the radar coverage area from the northwest at 0000 UTC. Precipitating cells within this storm evolved rapidly. A gust front appeared near the radar site at 0300 UTC and had echo cells stronger than 55 dBZ at its leading edge. At 0630 UTC, cloud clusters were distributed in an azimuthal sector from 260° to 60° (Fig. 2a). The three echo cells were labeled A, B, and C. Cell A was centered at $x = -65$ km, $y = 50$ km; cell B at $x = -15$ km, $y = 45$ km; and cell C at ($x = 25$ km, $y = 50$ km). By 0700 UTC (Fig. 2b), cell A had intensified with its maximum reflectivity changing from 30 dBZ to more than 35 dBZ. The intensity of cell C, however, had been reduced from 35 to 30 dBZ. A new cell, labeled as cell D at $x = 5$ km, $y = 45$ km, developed between cell B and cell C with its maximum reflectivity exceeding 35 dBZ. This observed decay, growth, and development of convective cells are typical of the evolution features occurring in most multicell storms.

The VVP analysis is performed to estimate low-level divergence, deformation, and wind vertical shear based on the velocity data sampled by the Carvel radar at 0630 UTC. Data preprocessing for velocity thresholding, unfolding, and removing outliers is similar to Koscielny

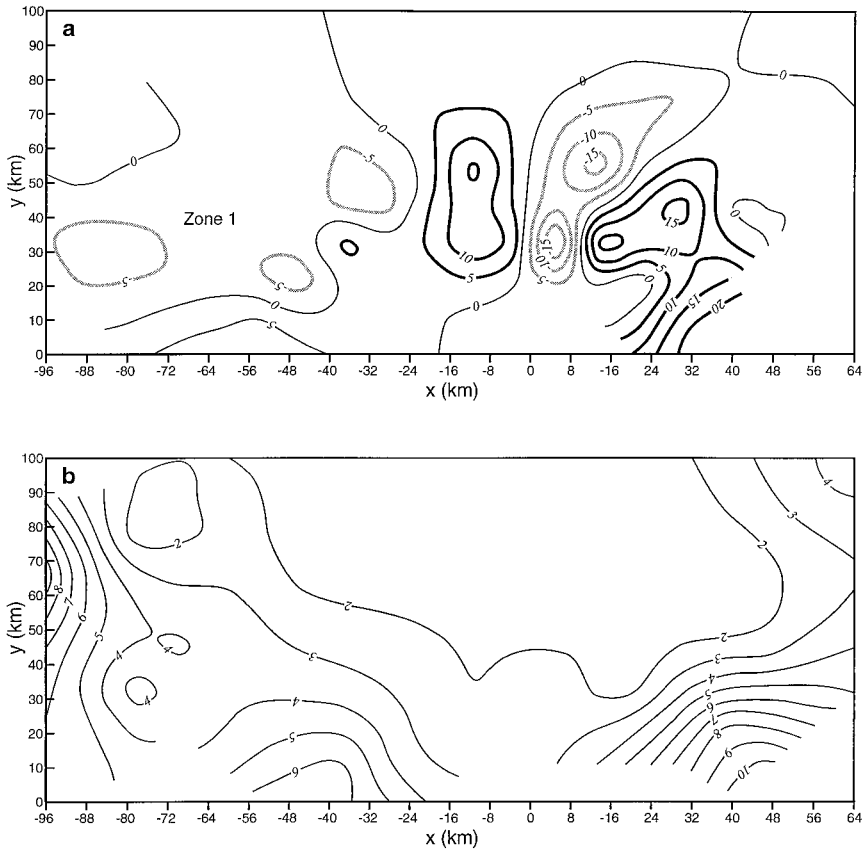


FIG. 3. The VVP results computed from Doppler velocity data at 0630 UTC for (a) divergence field contoured every $5 \times 10^{-4}$ s$^{-1}$; (b) standard error of divergence estimate, $\sigma_d$, contoured every $10^{-4}$ s$^{-1}$; (c) horizontal deformation, $(u_y + v_x)$, contoured every $2 \times 10^{-4}$ s$^{-1}$; and (d) vertical wind shear, $(u_z^2 + v_z^2)^{1/2}$, contoured every $2 \times 10^{-3}$ s$^{-1}$.

et al. (1982). Details are given in Xin (1996). After the data preprocessing, the corrected velocity data at ranges from 20 to 100 km and azimuths 260° to 60° are divided into a number of small sectors of size 40° × 20 km. The two lowest elevation angles of 0.5° and 1.5° are used. Values of divergence $(u_x + v_y)$, deformation $(v_x + u_y)$, and vertical shear $(u_z^2 + v_z^2)^{1/2}$ are estimated and plotted at the center of each sector. To obtain a better resolution, the analysis is repeated with the analysis sector shifted 10° in azimuth.

The VVP7-deduced divergence field at 0630 UTC is contoured in Fig. 3a. The results beyond a range of 100 km were neglected because of low signal-to-noise ratio. Similarly, the estimates at ranges less than 20 km are doubtful because of ground clutter contamination. The divergence appeared mainly in two large regions, centered at $x = -12$ km, $y = 45$ km and $x = 25$ km, $y = 45$ km, respectively. This divergent flow was likely associated with the precipitation outflow from the intense echoes (cells B and C shown in Fig. 2a). Meanwhile, there were two convergence zones in the northwestern (zone 1) and northern (zone 2) sectors, respectively. The magnitude of convergence in zone 2 exceeded $1.5 \times 10^{-3}$ s$^{-1}$. In zone 1, three small cells also had convergence values around $0.6 \times 10^{-4}$ s$^{-1}$. Our analysis supports the notion that low-level convergence triggers the development of convective cells (e.g., Ulanski and Garstang 1978).

Comparisons of Fig. 2 and Fig. 3a show that the enhancement of cell A (from 30 dBZ at 0630 to about 40 dBZ at 0700) was associated with the convergence area—Zone 1 at 0630 UTC. The strong convergence in zone 2 at 0630 led to a new large precipitating cell (cell D) at 0700 UTC. Conversely, echo cells in the divergent flow areas, that is, cells B and C, reduced their intensities during this 30-min period. This analysis confirms that the connection developed within regions of moderately strong convergence of about $10^{-4}$ s$^{-1}$ (e.g., Schreiber 1986; Wilson et al. 1992).

The standard error of divergence estimates $\sigma_d$, obtained from the VVP7 analysis at 0630 UTC, is plotted in Fig. 3b. The accuracy of the divergence estimate is of the order of $10^{-5}$ s$^{-1}$ in most areas. Such precision is needed for monitoring the convergence in convective

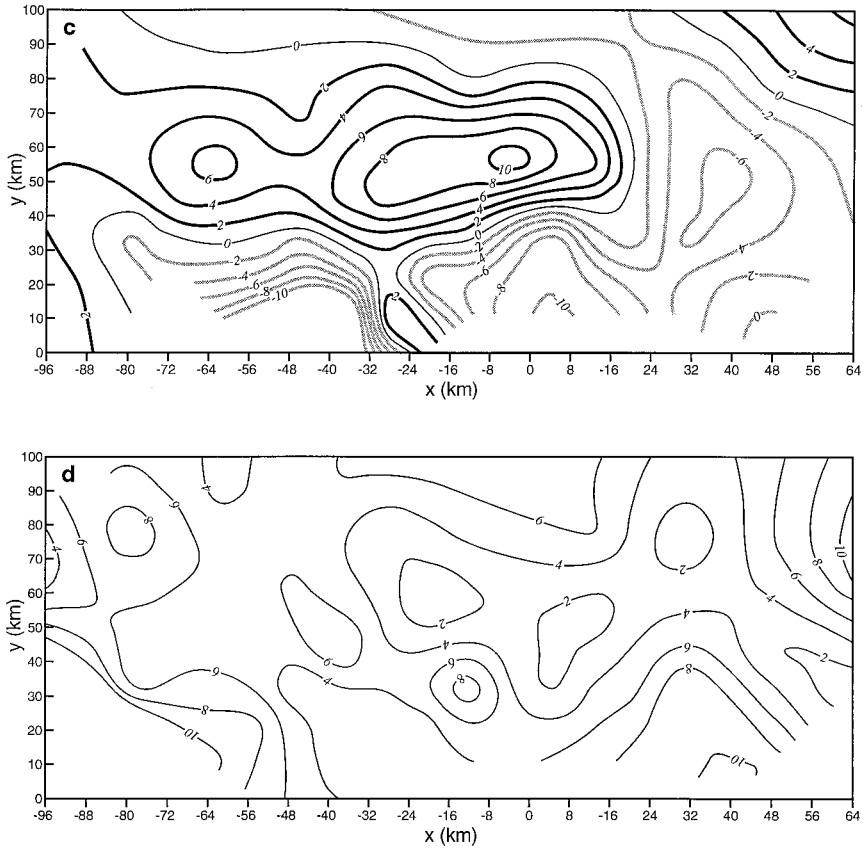


FIG. 3. (*Continued*)

storm conditions, which have typical magnitudes of about $10^{-4}$ s$^{-1}$ (e.g., Ulanski and Garstang 1978). For the three regions where $\sigma_d > 6.0 \times 10^{-5}$ s$^{-1}$, the divergence estimates become unreliable due to insufficient $V_r$ measurements when the detecting ranges were either larger than 90 km or smaller than 20 km, or the azimuths were beyond 60°.

Horizontal deformation and vertical shear were also retrieved using the VVP7 analysis. Three closed centers with strong deformation values (Fig. 3c) appeared where cells A, B, and C were located. Horizontal deformation reshaped the pattern of the precipitation field. Comparing Fig. 2 and Fig. 3c indicates that the positive deformation values dilated precipitation patterns northeastward, while precipitation areas with negative deformation values expanded along the northwest direction. The field of the VVP7-derived vertical shear at 0630 UTC is shown in Fig. 3d. In the two areas of divergence (apparent in Fig. 3a), vertical shear was strong with magnitudes reaching $8 \times 10^{-3}$ s$^{-1}$. The two convergence areas were also affected by vertical shear: $3 \times 10^{-3}$ s$^{-1}$ in zone 2 and $8 \times 10^{-3}$ s$^{-1}$ in zone 1. Echo cells were reduced in the divergence areas with strong vertical shear but were enhanced in the convergence regions with moderate-to-strong vertical shear.

## 4. Summary and conclusions

The accuracy of the VVP analysis is affected by the number of parameters included in the regression analysis. Comparison performed on a simulated wind field showed that divergence can be estimated accurately when the VVP method includes 7 wind parameters, but not when either 9 or 11 wind parameters are used. The 7 parameters include the divergence, deformation, vertical shear, and horizontal mean wind (modified by vertical vorticity). The analysis also showed that the size of analysis volumes affects the estimates. An appropriate analysis volume for estimating low-level divergence should have about 30°–40° azimuthal width and a 20–30-km range extent.

The seven-parameter VVP method was applied to the Doppler velocity data collected on 19 August 1992. The standard error of the divergence estimates was about $10^{-5}$ s$^{-1}$, or about one-tenth of the typical convergence magnitudes for storm formation. The initiation and enhancement of precipitating cells were associated with the low-level convergence that was estimated from the VVP analysis. On the other hand, echoes became suppressed in the areas of VVP-deduced divergence. Echo cells weakened in the divergent areas where strong wind shear appeared, but intensified when moderate-to-strong

wind shear was collocated with strong convergence. The results suggest that the VVP analysis technique has the potential for aiding in forecasting convective rainfall. Numerical simulation of this convective storm suggested that the timely knowledge of the convergence profile can improve the prediction of local rainfall (Xin and Reuter 1996). Current research is under way to examine more case studies in detail.

*Acknowledgments.* This research was supported by Environment Canada and the Natural Science and Engineering Research Council of Canada.

## REFERENCES

Browning, R. A., and R. Wexler, 1968: The determination of kinematic properties of a wind field using Doppler radar. *J. Appl. Meteor.*, **7,** 105–113.

Koscielny, A. J., R. J. Doviak, and R. M. Rabin, 1982: Statistical considerations in the estimation of divergence from single Doppler radar and application to pre-storm boundary-layer observation. *J. Appl. Meteor.*, **21,** 197–210.

Reuter, G. W., and R. Beaubien, 1996: Radar observations of snow formation in a warm pre-frontal snowband. *Atmos.–Ocean,* **34,** 605–626.

Schreiber, W. E., 1986: Case studies of thunderstorms initiated by radar-observed convergence lines. *Mon. Wea. Rev.,* **114,** 2256–2266.

Smith, S. D., and R. M. Rabin, 1989: Estimation of divergence in the prestorm boundary layer. *J. Atmos. Oceanic Technol.,* **6,** 459–475.

Ulanski, S. L., and M. Garstang, 1978: The role of surface divergence and vorticity in the life circle of convective rainfall. Part I: Observation and analysis. *J. Atmos. Sci.,* **35,** 1047–1062.

Waldteufel, P., and H. Corbin, 1979: On the analysis of single Doppler radar data. *J. Appl. Meteor.,* **18,** 532–542.

Wilson, J. W., and W. E. Schreiber, 1986: Initiation of convective storms at radar-observed boundary-layer convergence lines. *Mon. Wea. Rev.,* **114,** 2516–2536.

——, G. B. Foote, N. A. Crook, J. C. Fankhauser, C. G. Wade, J. D. Tuttle, C. K. Mueller and S. K. Kruger, 1992: The role of boundary-layer convergence zones and horizontal rolls in the initiation of thunderstorms: A case study. *Mon. Wea. Rev.,* **120,** 1785–1815.

Xin, L., 1996: Effects of mesoscale convergence on convective and stratiform rainfall: Radar observations and numerical simulations. Ph.D. dissertation, University of Alberta, 178 pp. [Available from Library, Dept. of Earth and Atmospheric Sciences, University of Alberta, Edmonton, AB T6G 2E3, Canada.]

——, and G. W. Reuter, 1996: Numerical simulation of the effects of mesoscale convergence on convective rain showers. *Mon. Wea. Rev.,* **124,** 2828–2842.